This work was published in the journal Geology in 2018, with doi 10.1130/G39916.1

Landslide-driven drainage divide migration

Maxwell P. Dahlquist, A. Joshua West, and Gen Li

Department of Earth Sciences, University of Southern California, Los Angeles, California 90089, USA

ABSTRACT

Drainage divide migration reorganizes river basins, redistributing erosive energy and contributing to feedbacks between tectonics, erosion, and climate. However, the conditions governing divide migration and the time scales on which it occurs are poorly understood. By connecting channels to hillslopes in steep landscapes, landslides are expected to play a central role in divide migration and landscape evolution. In this study, we examine landslides triggered by three events (two earthquakes and a tropical cyclone), seeking insight into controls on divide migration. Of the ~100,000 landslides triggered, we mapped 365 that caused a divide to migrate, resulting in a total exchange of ~2 km^2 between basins from ~82,000 km^2 affected by landsliding. By applying several proposed metrics for divide stability based on river channel morphology, we use our database of divide migrations to test for the role of landslides in coupling between channels and divides. We find that, at the time scale of a single landslide-generating event, patterns of area gain and loss between basins are consistent with landscapes progressing toward steady state, as inferred from channel metrics. We also propose a metric to quantify divide migration, area exchange, and the contribution of an event toward topographic steady state. Restricting our analysis to the main drainage divide, and using estimates of recurrence interval and the rate of topographic evolution in Taiwan, we calculate that

landslides triggered by large typhoons account for a minimum of 12%–15% of southern Taiwan's progress toward steady state.

INTRODUCTION

Fluvial erosion is a primary force shaping most landscapes on Earth (Strahler, 1952; Whipple and Tucker, 1999), countering and influencing uplift by mobilizing and redistributing mass (Whipple, 2009). A river's discharge determines, in part, its ability to erode bedrock, and is controlled by the area of its drainage basin and the precipitation it receives (Hack, 1957). The positions of drainage divides, and thus basin area, are not fixed over time. Divides are thought to migrate via coupling between rivers and hillslopes: river incision generates oversteepened hillslopes, which fail during landslides, occasionally breaching a ridge and causing one basin to gain area at another's expense (Burbank et al., 1996; Harvey, 2001; Hovius et al., 1998; Larsen and Montgomery, 2012) (Fig. 1). Over time, this process should drive tectonically active landscapes toward steady state, where erosion rates are balanced across divides (Whipple and Tucker, 1999; Willett and Brandon, 2002; Whipple, 2009).

Despite the accepted importance of drainage divide migration in shaping tectonically active landscapes, this process remains poorly understood, with few direct observations (Bonnet, 2009). Landslide-generating events, such as strong earthquakes and extreme storms, offer natural experiments for observing divide migration processes in action. The goal of this study is to examine the results of these experiments, using high-resolution satellite imagery and digital elevation models (DEMs) to identify pre- and post-event divide locations.

River channels span most of the relief in drainage basins and control basin geometry (Whipple and Tucker, 1999). Recent studies have explored topographic metrics for divide instability (Willett et al., 2014; Whipple et al., 2017) and have identified relationships between divide migration and river profile morphology (Yang et al., 2015; Whipple et al., 2017). These studies have been based predominantly on landscape evolution model outputs and inferences from river profile analysis. Empirical observations offer the opportunity to test these results directly and to isolate the effect of landslides in coupling river channels to divides. In this paper, we quantify divide migration in three locations and find that patterns of area gain and loss generally result in divides progressing toward steady state, as predicted by channel and basin geometry. We use this information to attempt to quantify the impact of storm-triggered landslides on the long-term evolution of the Central Range in Taiwan.

STUDY AREAS

Large earthquakes in Wenchuan, China, and central Nepal, and a typhoon in southern Taiwan, together triggered more than 10^5 landslides, a subset of which caused divide migration (Fig. 1). All three events affected steep, mountainous terrain. The M_w 7.9 2008 Wenchuan earthquake struck central China on 12 May 2008. Strong shaking generated more than 60,000 landslides (Li et al., 2014). The M_w 7.8 Gorkha earthquake struck central Nepal on 25 April 2015 and caused ~25,000 mapped landslides (Roback et al., 2017). Typhoon Morakot made landfall in Taiwan on 7 August 2009. The most destructive effect of Typhoon Morakot was its heavy rainfall, up to nearly 3 m between 7 and 9 August. This rainfall generated more than 20,000 landslides in the steep Central Range of southern Taiwan (Lin et al., 2011). The Taiwan data set is particularly useful in evaluating divide migration for several reasons: the landslide density was high, image and DEM quality are good over all affected areas, and independent estimates of the progression of the Central Range toward topographic steady state allow us to view our divide migration data within the context of long-term landscape evolution (Stolar et al., 2007).

LANDSLIDE MAPPING

We mapped ridge-breaching landslides visually using Google Earth Pro™ and measured the area captured by each landslide. Google Earth uses Shuttle Radar Topography Mission (SRTM) 30 m topography where available, filling in areas with limited coverage or poor data quality with other DEMs. The advantage of Google Earth is that the three-dimensional terrain projection simplifies the identification of instances of divide migration. The topography predates the events, resulting in ridge-breaching landslides appearing draped over the ridge (Fig. 1). We assumed the uppermost extent of the scarp represents the new divide. In both the satellite images and in field observations from all three locations, we found that most landslides that appear to initiate at the ridge (see Densmore and Hovius, 2000) actually initiate a few meters below it, and do not cause divide migration. We included only landslides that clearly breach a ridge, which comprise only a fraction of the total number that initiate near ridges.

Proper image positioning and rectification is critical for this method. Some misalignments are visible in Google Earth imagery, so we verified that ridges included in this study are properly georeferenced to ridges in the DEM. To do this, we used ridges that are easily identifiable by shadows or, where ridges were not clearly identifiable in images, we checked that nearby streams are correctly located with respect to topographic minima (Figs. DR1 and DR2 in the GSA Data Repository[1]). This process enables us to exclude areas where divide locations are suspect; comprising roughly 10% of the total landslide affected area. We mapped landslides specifically for this study because we found that using polygons from existing landslide inventories yielded significantly less accurate georeferencing of landslides with respect to ridges.

TOPOGRAPHIC ANALYSIS

While landslides are a hillslope process, and locations of landslides may be controlled by local slope, ground shaking, fluid flow, and other factors (Montgomery and Dietrich, 1994), we focus on river incision as a driver of landsliding through oversteepening of hillslopes. River incision is thought to be a primary driver of drainage basin evolution (Whipple and Tucker, 1999), so to contextualize the data on divide migrations and to test for the role of landslides in river-divide coupling, we analyzed rivers draining basins affected by divide migration. We calculated topographic metrics proposed to capture information about divide stability: χ (chi), upstream-averaged local relief, and upstream-averaged channel gradient, all of which may indicate cross-divide differences in erosion rate (Willett et al., 2014; Whipple et al., 2017). The detachment-limited stream power model relates the change in the elevation of a channel to its slope and drainage area (Howard et al., 1994):

$$\frac{\partial z}{\partial t} = U(x,t) - K(x,t)A^{m}\left|\frac{\partial z}{\partial x}\right|^{n}, \qquad (1)$$

where z is elevation, *t* is time, U is rock uplift rate, K is erodibility, A is upstream drainage area, x is distance upstream, and m and n are constants modifying area and slope, whose values may vary under different conditions. Transient landscapes are expected to evolve toward a state where uplift is balanced by erosion (Whipple and

Tucker, 1999; Willett and Brandon, 2002). Based on this stream power model, Perron and Royden (2013) proposed the χ (chi) metric, an integral of drainage area along a river, for the interpretation of bedrock river profiles:

$$\chi = \int_{x_b}^{x} \left(\frac{A_0}{A}\right)^{\frac{m}{n}} dx \,, \qquad (2)$$

where x_b is a point on the channel at base level, and A_0 is a reference drainage area that gives chi dimensions of length. In principle, steady-state divides should have equal χ values on either side. Differences in χ values across divides are expected to reflect divide instability, with a lower-χ stream expected to capture area from a higher-χ stream (Willett et al., 2014). However, the interpretation of χ differences across divides may be complicated by spatial and temporal variations in U and K, which are poorly constrained in many regions (Whipple and Tucker, 1999).

Streams were defined and fluvial metrics calculated using the TopoToolbox 2 and DivideTools functions for Matlab using SRTM topographic data (Schwanghart and Scherler, 2014; Forte, 2016). We used 1 km^2 as the minimum drainage area to define a stream, and a standard reference concavity of 0.45. We set base level to 700 m in Wenchuan (the elevation of the Sichuan basin, which clearly demarcates the bedrock-alluvial transition), and 500 m in Nepal, where many rivers of interest enter basins or begin to widen and form alluvial valleys. In Taiwan, we calculated χ values both by assuming base level is sea level, as well as defining base level individually for each basin by visually identifying the bedrock-alluvial transition; both of which yielded nearly identical results.

We calculated local relief using a radius of 500 m, which does not exceed the average hillslope length. Channel gradient was calculated for segments of varying length with a minimum of 10 m vertical drop.

For each instance of divide migration we identified, we compared the metrics of the river that gained drainage area with those of the river that lost area. If landslides are driving the landscape toward steady state, we expect to see the majority of divide migrations characterized by gain in area of rivers with lower χ, higher relief, and high gradient (Willett et al., 2014; Whipple et al., 2017). To evaluate this hypothesis, we compared values of χ, upstream-averaged local relief, and upstream-averaged gradient at the point along a stream with the most direct flow path from the affected divide.

RESULTS

We found a total of 365 instances of divide migration, with 56 caused by the Gorkha earthquake, 156 by the Wenchuan earthquake, and 153 by Typhoon Morakot. From these three events, we measured 1.857 ± 0.49 km^2 of total drainage area exchanged: 1.248 ± 0.245 km^2 in the Wenchuan earthquake, 0.552 ± 0.211 km^2 in Typhoon Morakot, and 0.068 ± 0.035 km^2 in the Gorkha earthquake (reported uncertainties include estimates of the error introduced by the ~30 m DEM resolution, further examined in the Data Repository, Figure DR3). A single large landslide triggered by the Wenchuan earthquake affected four divides and was alone responsible for 0.71 km^2 of area exchange.

61.4% of migration directions were toward steady state, as predicted by relief differences ($p = 8.18 \times 10^{-6}$, where p is the probability that migration direction is irrespective of the metric), 58.7% by gradient ($p = 5.72 \times 10^{-4}$), and 56.4% by χ ($p = 7.97 \times 10^{-3}$). Local relief and channel gradient better predict divide migration than x differences when compared across transient divides in simulations (Whipple et al., 2017) as well as in this data set (Table 1). Overall, divide migrations are roughly normally distributed with respect to differences in χ, relief, and gradient (Fig. 2). The amount of area captured in each landslide does not appear to be dependent on fluvial geometry, i.e., larger landslides are not necessarily associated with larger differences in relief, gradient, or x across divides. Cross-divide differences in mean local relief and mean gradient are similar at each affected divide, but gradients in x are only weakly correlated with gradients in the other two metrics (Fig. DR4).

DISCUSSION

Landslides Drive Divides Toward Steady State

The results of this study show that event-triggered landslides measurably drive a landscape toward steady state with respect to the river network. This indicates that, even on the time scale of an earthquake or storm, mobility of divides is conditioned by river incision, and thus incision can be coupled to hillslopes and divides by landslides. These links have been inferred in prior studies (e.g., Stark, 2010; Buscher et al., 2017) but not conclusively demonstrated with the kind of direct empirical evidence provided here.

Mean local relief may predict divide migration well because it is essentially a coarse measure of hillslope angle. Higher-resolution topographic data than the 30 m SRTM could allow the effects of local slope to be disentangled from channel geometry, further clarifying relationships between channels and divide migration. Tributary capture may be important in basin reorganization on similar time scales, but we do not identify any instances of tributary capture in these events.

The lack of any strong relationship between χ and the other metrics (Fig. DR4) highlights the difficulty in choosing a proxy for basin stability. In Nepal and Taiwan, χ disparities do not predict the direction of divide migration, but for the Wenchuan earthquake, χ outperforms the other metrics (Table 1). The reason for this difference is not immediately obvious, but may suggest that river incision better conforms to the stream power model, upon which the χ calculation is based, in the Wenchuan region. Interpretation of metrics that depend on the stream power model may be complicated by nonuniform uplift and erodibility. Additionally, because χ is an integral from base level, including downstream geometry of a basin, it may be better suited to examining broad, regional trends rather than area exchange between first-order basins.

A Metric for Divide Migration

Drainage divides, like coastlines, have a fractal character, making linear measurements scale-dependent (Rodríguez-Iturbe and Rinaldo, 2001). We propose a metric for the mobility of drainage divides and the geometric transience of landscapes that is independent of linear divide migration rates:

$$\mathrm{n_r} = \frac{\mathrm{A_e}/\mathrm{A_t}}{t}, \quad (3)$$

where the reorganization number, $\mathrm{n_r}$, is defined as the ratio of the area exchanged in a divide migration event $\mathrm{A_e}$ to the total area of the affected landscape $\mathrm{A_t}$, divided by the characteristic time scale, *t*, of divide migration events. This yields an absolute measure of divide mobility, not considering progression toward steady state, and irrespective of the scale of the affected basins. For divide migrations triggered by Typhoon Morakot, we calculate $\mathrm{n_r} = 1.04 \times 10^{-6}\ \mathrm{yr}^{-1}$ based on a minimum recurrence interval (*t*) of 200 yr (West et al., 2011), A_e of 0.541 km^2, and A_t of 2.6×10^3 km^2. This n_r value represents the fraction of area in a landscape that is exchanged between basins of any order during the time scale of interest. For Wenchuan, given *t* of 2300–3300 yr for large earthquakes on the Longmenshan Fault Zone (Ran et al., 2010), A_e of 1.294 km^2, and A_t of 4.0×10^3 km^2 yields $n_r = 1.4 \times 10^{-7}$ yr^{-1} to 9.8×10^{-8} yr^{-1}. Events with different recurrence intervals may cause divide migration in the same landscapes, but n_r may be useful for quantifying a single event's influence on a landscape, and the overall motility of divides in a landscape. The higher value of n_r for Taiwan compared to Wenchuan implies comparatively more rapid reorganization of this landscape during the single events studied here. Moreover, these events are likely to occur more frequently in Taiwan: the recurrence interval for large earthquakes in Taiwan is ~475 yr (Cheng et al., 2007) versus 2300–3300 yr for the Longmenshan Fault Zone, while Taiwan also experiences greater rainfall erosivity (Panagos et al., 2017).

While there is much debate as to whether arc-continent collision and orogeny in Taiwan is progressing from north to south (Suppe, 1981) or occurring simultaneously along strike (Lee et al. 2015), the topography of the southernmost 125 km of Taiwan along strike (A_t ~4,250 km^2 area) appears not to have achieved steady state. Stolar et al. (2007) estimated a duration t of 1.8–2.3 m.y. from subaerial exposure to steady-state topography. We assume that steady state is achieved by migration of the main divide, and its steady-state position lies between its current easternmost and westernmost extents in the southern Central Range (Fig. 3). To obtain a *maximum* estimate of area that must be exchanged between east- and west-flowing basins to achieve steady state, we assume that the divide must migrate from one extreme to the other. Between the hypothetical easternmost and westernmost divide positions, we measure A_e ~1,133 km^2. We find the maximum n_r required for the main divide to reach steady state in 1.8–2.3 m.y. is 1.2–1.5 $\times 10^{-7}$ yr^{-1}. Nine of 153 Typhoon Morakot migrations occurred on the main divide, with an average area captured of 3600 m^2. Assuming 64% of migrations result in progress toward steady state (Table 1, from the value for relief) yields n_r of 1.8×10^{-8} yr^{-1}. Comparing this value to n_r = 1.2–1.5 $\times 10^{-7}$ yr^{-1} estimated for the long term means that Morakot-type landslides account for a minimum of 12%–15% of the motion of the main divide toward steady state. Tributary capture and other landslide-generating events such as earthquakes may also contribute to migration of the central divide. We emphasize that this calculation is based on a small landslide population and that we use a maximum estimate of the amount of necessary area exchange. The role of typhoon-triggered landslides may thus be more important than we estimate, but this method could provide an approach for more robustly evaluating the role of landslides given data from a larger number of events.

CONCLUSIONS

By examining ridge-breaching landslides triggered by three recent events, we have demonstrated that event-triggered landslides couple river channels to hillslopes and ridges, and lead to migration of drainage divides toward steady state. A landscape's progress toward steady state is thus measurable at the time scale of one earthquake or storm. We compared three channel morphology proxies for the direction a divide will migrate to achieve steady state: χ, mean local relief, and mean channel gradient. All three meaningfully predict the direction of observed migrations. χ is an excellent predictor for Wenchuan migrations, but does not perform as well in the other areas. Cross-divide differences in relief and gradient closely correspond for all three sites, while differences in χ are weakly correlated with the other two metrics.

We propose a reorganization number as a metric for divide mobility, helping to quantify the impact of a landsliding event on a landscape. Applying this approach to southern Taiwan, where the progression of the landscape toward steady state has been widely discussed, we find that typhoons on the scale of Morakot are likely responsible for a minimum of 12%–15% of the motion of the main divide in the Central Range toward a steady-state position.

ACKNOWLEDGMENTS

This work was supported by National Science Foundation grants EAR-1546630 and EAR-1250214. Dahlquist received support from a University of Southern California Provost's Fellowship. We thank three reviewers for constructive comments that considerably improved the manuscript, and Mark Quigley for editorial handling.

REFERENCES CITED

Bonnet, S., 2009, Shrinking and splitting of drainage basins in orogenic landscapes from the migration of the main drainage divide: Nature Geoscience, v. 2, p. 766–771, https://doi.org/10.1038/ngeo666.

Burbank, D.W., Leland, J., Fielding, E., Anderson, R.S., Brozovic, N., Reid, M.R., and Duncan, C., 1996, Bedrock incision, rock uplift and threshold hillslopes in the northwestern Himalayas: Nature, v. 379, p. 505–510, https://doi.org/10.1038/379505a0.

Buscher, J., Ascione, A., and Valente, E., 2017, Decoding the role of tectonics, incision and lithology on drainage divide migration in the Mt. Alpi region, southern

Apennines, Italy: Geomorphology, v. 276, p. 37–50, https://doi.org/10.1016/j.geomorph.2016.10.003.

Cheng, C.-T., Chiou, S.-J., Lee, C.-T., and Tsai, Y.-B., 2007, Study on probabilistic seismic hazard maps of Taiwan after Chi-Chi earthquake: AGH Journal of Mining and Geoengineering, v. 2, p. 19–28.

Densmore, A.L., and Hovius, N., 2000, Topographic fingerprints of bedrock landslides: Geology, v. 28, p. 371–374, https://doi.org/10.1130/0091-7613(2000)28<371:TFOBL>2.0.CO;2.

Forte, A., 2016, DivideTools: Set of Matlab-based tools for analyzing drainage divide stability: https://github.com/amforte/DivideTools.

Hack, J.T., 1957, Studies of longitudinal stream profiles in Virginia and Maryland: U.S. Geological Survey Professional Paper, Number. 294-B, p. 45–97.

Harvey, A., 2001, Coupling between hillslopes and channels in upland fluvial systems: Implications for landscape sensitivity, illustrated from the Howgill Fells, northwest England: Catena, v. 42, p. 225–250, https://doi.org/10.1016/S0341-8162(00)00139-9.

Hovius, N., Stark, C., Tutton, M., and Abbott, L., 1998, Landslide-driven drainage network evolution in a pre-steady-state mountain belt: Finisterre Mountains, Papua New Guinea: Geology, v. 26, p. 1071–1074, https://doi.org/10.1130/0091-7613(1998)026<1071:LDDNEI>2.3.CO;2.

Howard, A.D., Dietrich, W.E., and Seidl, M.A., 1994, Modeling fluvial erosion on regional to continental scales: Journal of Geophysical Research: Solid Earth, v. 99, B7, p. 13971–13986, https://doi.org/10.1029/94JB00744.

Larsen, I.J., and Montgomery, D.R., 2012, Landslide erosion coupled to tectonics and river incision: Nature Geoscience, v. 5, p. 468–473, https://doi.org/10.1038/ngeo1479.

Lee, Y.-H., Byrne, T., Wang, W.-H., Lo, W., and Rau, R.-J., 2015, Simultaneous mountain building in the Taiwan orogenic belt: Geology, v. 43, p. 451–454, https://doi.org/10.1130/G36373.1.

Li, G., West, A.J., Densmore, A.L., Jin, Z., Parker, R.N., and Hilton, R.G., 2014, Seismic mountain building: Landslides associated with the 2008 Wenchuan earthquake in the context of a generalized model for earthquake volume balance: Geochemistry Geophysics Geosystems, v. 15, p. 833–844, https://doi.org/10.1002/2013GC005067.

Lin, C.-W., Chang, W.-S., Liu, S.-H., Tsai, T.-T., Lee, S.-P., Tsang, Y.-C., Shieh, C.-L., and Tseng, C.-M., 2011, Landslides triggered by the 7 August 2009 Typhoon Morakot in southern Taiwan: Engineering Geology, v. 123, p. 3–12, https://doi.org/10.1016/j.enggeo.2011.06.007.

Montgomery, D.R., and Dietrich, W.E., 1994, A physically based model for the topographic control on shallow landsliding: Water Resources Research, v. 30, p. 1153–1171, https://doi.org/10.1029/93wr02979.

Panagos, P., et al., 2017, Global rainfall erosivity assessment based on high-temporal resolution rainfall records: Scientific Reports, v. 7, https://doi.org/10.1038/s41598-017-04282-8.

Perron, J.T., and Royden, L., 2013, An integral approach to bedrock river profile analysis: Earth Surface Processes and Landforms, v. 38, p. 570–576, https://doi.org/10.1002/esp.3302.

Ran, Y., Chen, L., Chen, J., Wang, H., Chen, G., Yin, J., Shi, X., Li, C., and Xu, X., 2010, Paleoseismic evidence and repeat time of large earthquakes at three sites along the Longmenshan fault zone: Tectonophysics, v. 491, p. 141–153, https://doi.org/10.1016/j.tecto.2010.01.009.

Roback, K., and Clark, M.K., West, A.J., Zekkos, D., Li, G., Gallen, S.F., Chamlagain, D., and Godt, J.W., 2017, The size, distribution, and mobility of landslides caused by the 2015 M_w7.8 Gorkha earthquake, Nepal: Geomorphology, https://doi.org/10.1016/j.geomorph.2017.01.030.

Rodríguez-Iturbe, I., and Rinaldo, A., 2001, Fractal River Basins: Chance and Self-Organization: Cambridge, UK, Cambridge University Press, 570 p.

Schwanghart, W., and Scherler, D., 2014, TopoToolbox 2—MATLAB-based software for topographic analysis and modeling in Earth surface sciences: Earth Surface Dynamics, v. 2, p. 1–7, https://doi.org/10.5194/esurf-2-1-2014.

Stark, C.P., 2010, Oscillatory motion of drainage divides: Geophysical Research Letters, v. 37, https://doi.org/10.1029/2009GL040851.

Stolar, D.B., Willett, S.D., and Montgomery, D.R., 2007, Characterization of topographic steady state in Taiwan: Earth and Planetary Science Letters, v. 261, p. 421–431, https://doi.org/10.1016/j.epsl.2007.07.045.

Strahler, A.N., 1952, Dynamic basis of geomorphology: Geological Society of America Bulletin, v. 63, p. 923, https://doi.org/10.1130/0016-7606(1952)63[923:DBOG]2.0.CO;2.

Suppe, J., 1981, Mechanics of mountain building and metamorphism in Taiwan: Memoirs of the Geological Society of China, v. 4, p. 67–89.

West, A.J., Lin, C.-W., Lin, T.-C., Hilton, R.G., Liu, S.-H., Chang, C.-T., Lin, K.-C., Galy, A., Sparkes, R.B., and Hovius, N., 2011, Mobilization and transport of coarse woody debris to the oceans triggered by an extreme tropical storm: Limnology and Oceanography, v. 56, p. 77–85, https://doi.org/10.4319/lo.2011.56.1.0077.

Whipple, K.X, and Tucker, G.E., 1999, Dynamics of the stream-power river incision model: Implications for height limits of mountain ranges, landscape response timescales, and research needs: Journal of Geophysical Research: Solid Earth, v. 104, B8, p. 17661–17674, https://doi.org/10.1029/1999JB900120.

Whipple, K.X, 2009, The influence of climate on the tectonic evolution of mountain belts: Nature Geoscience, v. 2, p. 97–104, https://doi.org/10.1038/ngeo413.

Whipple, K.X, Forte, A.M., Dibiase, R.A., Gasparini, N.M., and Ouimet, W.B., 2017, Timescales of landscape response to divide migration and drainage capture: Implications for the role of divide mobility in landscape evolution: Journal of Geophysical Research: Earth Surface, v. 122, p. 248–273, https://doi.org/10.1002/2016JF003973.

Willett, S.D., and Brandon, M.T., 2002, On steady states in mountain belts: Geology, v. 30, p. 175, https://doi.org/10.1130/0091-7613(2002)030<0175:OSSIMB>2.0.CO;2.

Willett, S. D., S. W. Mccoy, J. T. Perron, L. Goren, and C.-Y. Chen, 2014, Dynamic reorganization of river basins: Science, v. 343, https://doi.org/10.1126/science.1248765.

Yang, R., Willett, S.D., and Goren, L., 2015, In situ low-relief landscape formation as a result of river network disruption: Nature, v. 520, p. 526–529, https://doi.org/10.1038/nature14354.

FIGURE CAPTIONS

Figure 1. A landslide in southern Taiwan (from Google Earth™). Divide migration occurs when a landslide breaches a ridge, causing the divide to move to a new position at the top of the slip surface. Rivers are color-coded by upstream-averaged local relief. In this case, the higher-relief basin captures area, consistent with a divide progressing toward steady state. This is one of the larger migration events we documented, capturing ~11,000 m^2.

Figure 2. Histograms of divide migrations and area capture plotted by difference in cross-divide metrics. For consistency with the other two metrics, we reverse the sign of χ (chi) differences. Positive differences in metrics indicate progress toward steady state. Solid lines show numbers of migration instances broken down by site; dashed lines and shaded histogram show areas for all sites together. We do not include the largest Wenchuan (China) landslide in the area capture measurement, as it caused ~0.7 km^2 to be exchanged.

Figure 3. Map of divide migrations used in this study. Main divide of Taiwan Central Range plotted in red; hypothetical eastern and western divides used in n_r calculation in black. A: Nepal. B: Taiwan. C: Wenchuan, China.

GSA Data[1] Repository item 2018xxx, additional figures (Figs. DR1–DR5) describing our methods and error calculations in greater detail, is available online at http://www.geosociety.org/datarepository/2018/, or on request from editing@geosociety.org.

Table 1. divide migration statistics

				% of area captured			% of divide migrations		
Event	Number of migrations	Area exchanged (km^2)	± (km^2)	By lower chi river	By higher gradient river	By higher relief river	Lower chi gains area	Higher gradient gains area	Higher relief gains area
Wenchuan	156	1.248	0.245	68.1	56.3	44.7	64.7	56.9	56.8
Nepal	56	0.068	0.035	55.2	61.8	66.3	49.7	60.7	66.7
Taiwan	153	0.541	0.221	47.2	59.2	65.6	50.3	59.9	64.2
Total	365	1.857	0.491	61.5	57.3	51.6	56.4	58.7	61.4

Figure 1

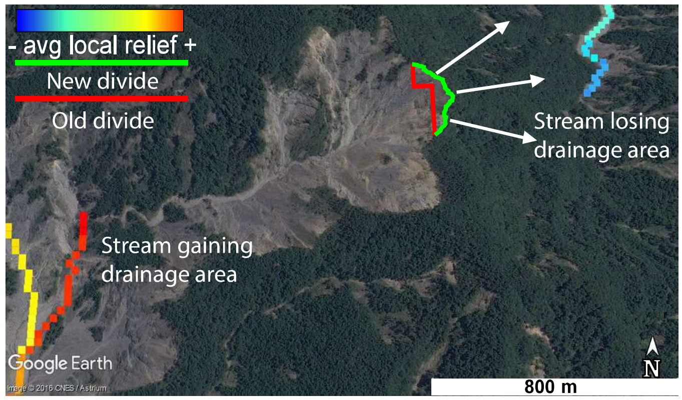

Figure 2

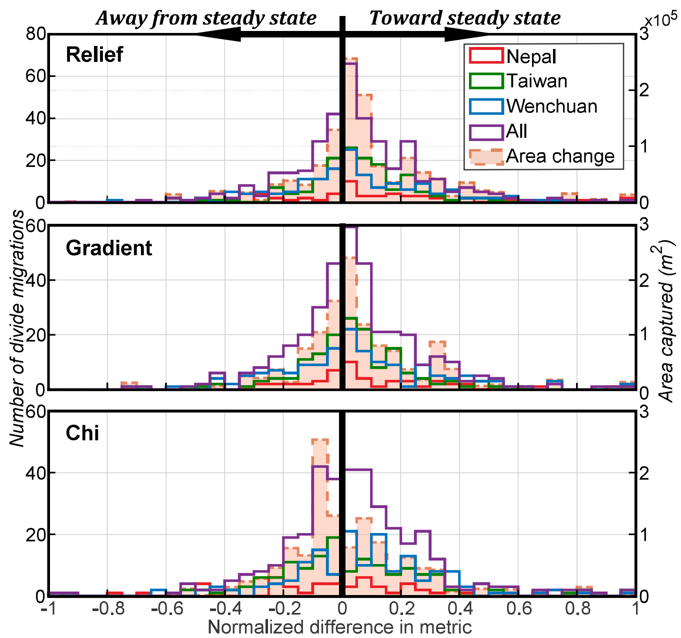

Figure 3

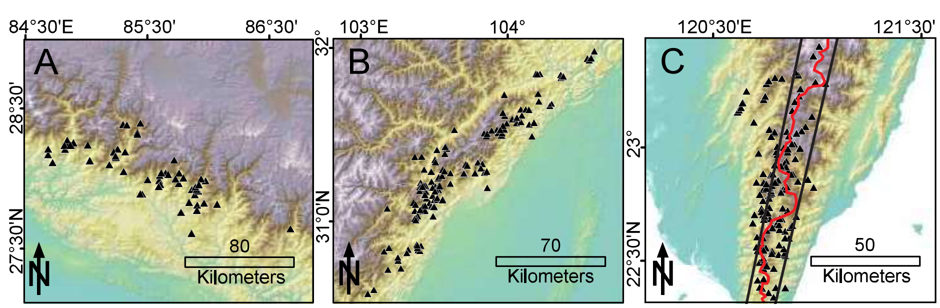

Supplementary Information for "Landslide-driven drainage divide migration"

Maxwell P. Dahlquist, A. Joshua West, and Gen Li

VERIFYING GEOLOCATION OF RIDGES

For our method of mapping divide migrations to be valid, ridges in photos must be properly georeferenced to ridges in the topography. Google Earth has some known issues with georeferencing and orthorectification in some areas that can cause mismatching between images and topography. Ridges are identifiable in satellite images where the sun angle generates appropriate shadows (Figure DR1), or where a vegetation contrast or cliff edge is apparent, and we used the correspondence of these visible ridges with the Google Earth base topography to confirm accurate referencing for the areas analyzed in this study, where possible.

Verifying the location of ridges in this manner was not possible in all images. A more widely applicable method for verifying that images are properly georeferenced is checking that streams are properly placed at the lowest points of valleys (Figure DR2). We assume that when streams are properly georeferenced, ridges are as well, such that our divide migration mapping method is reasonable to use where streams are in place. To determine whether this assumption is valid, we examine locations in our three field areas where ridges are clearly visible, and verify that both the ridge and the adjacent streams are properly georeferenced. In steep valleys, a 30-meter resolution DEM sometimes fails to capture all the fine meanders of small streams, but we find this does not necessarily indicate a poorly georeferenced image. Rather, it is a systematic displacement of the stream out of a topographic low that indicates a problematic area where ridge locations are untrustworthy. We checked more than 150 locations where ridges are clearly visible and found only 2 where streams are properly located but ridges are out of place. Figure

DR2 shows an example of a properly located ridge flanked by two properly located streams. Given the good correspondence between properly referenced streams and ridges, we used in-place streams to screen areas of accurately referenced imagery for use in our analysis.

ERROR INTRODUCED BY DEM RESOLUTION

Since we calculate the amount of area captured by a landslide using the position of the ridge before the landslide occurred and define the position of that ridge based on the topography, error is introduced due to the 30-meter resolution of the DEM. The satellite photos used to identify the top of the landslide scarp have a resolution of 0.5-2 meter, so the error introduced in the area calculation by photo resolution is negligible by comparison.

We have already introduced our method for ensuring that satellite imagery is properly geolocated to the topography, and we excluded areas from our analysis where imagery was not accurately georeferenced. We thus estimate error based on properly located ridges. While ridges are not linear features, at the scale of an individual landslide we find it is a reasonable approximation to define the actual ridge as a line. To estimate the error introduced by the DEM resolution, we wish to calculate the area between the DEM-defined ridge and the actual ridge.

Approximating the location of a ridge using a 30-meter DEM results in a ridge defined by a series of points $p_0, p_1, \ldots, p_n$ spaced 30 meters apart, each of which is a distance x_n from the actual ridge (Figure DR3). The area between a DEM-defined ridge of length l and the actual ridge it describes is defined:

$$a_e = \sum_{n=0}^{l/r} \left(\frac{x_{n-1}+x_n}{2}\right)\sqrt{r^2-(|x_{n-1}-x_n|)^2}, \quad (1)$$

where r is the resolution of the DEM. For a correctly located ridge, maximum distance x for any point p is:

$$x_{max} = \sqrt{\frac{r^2}{2}}. \quad (2)$$

x_{min} is zero for a point that lies on the actual ridge. For a 30-meter DEM, we find an average x of 10.61 meters.

For each field area, we measure the total length of affected divide l and find 19,900 meters for Taiwan, 23,100 meters for Wenchuan, and 3,300 for Nepal. Applying equation 1, we obtain error estimates for our area capture calculations for each site: 1.248±0.245 km^2, 0.541±0.211 km^2, and 0.068±0.035 km^2, respectively.

SUPPLEMENTAL FIGURE CAPTIONS

Figure DR1. Ridge identification by shadow. Images show a ridge in Taiwan before (2001) and after (2011) Typhoon Morakot, in the top and bottom panels, respectively. The ridge in the top photo is easily identified by the shadow it casts, making the divide migration caused by the landslide in the bottom image easily identifiable even without using topographic data. Throughout the study regions, we used similar instances of visibly well-defined ridges to check for accurate positioning of images with respect to topography.

Figure DR2. Geolocation of ridges and rivers. Image shows a ridge and adjacent river valleys in Taiwan (top) and an elevation profile of the path marked in blue. Image and topography are both from Google Earth. The ridge and rivers are marked with arrows of corresponding colors in the image and elevation profile. The imagery and topography in this area are properly georeferenced. Similar evaluations were used to screen accurate georeferencing in all three study regions.

Figure DR3. Schematic of uncertainty in area calculations introduced by DEM resolution. In the error calculation, p_n is represented by the centers of the brown squares. The distance between p_n and the actual ridge shown in red is x_n.

Figure DR4. Cross-divide differences in chi, relief, and gradient plotted against each other. Each point represents the difference in metrics for a single divide migration site. The strong correlation between relief and gradient is indicative that both metrics represent straightforward measures of basin geometry, i.e., a basin where rivers have a steep gradient should also have high relief as well. Calculating chi involves more assumptions and considers downstream geometry, which may lead to the lack of correlation with the other two metrics.

Figure DR5. Maps of relief, gradient, and chi plotted along rivers in study areas. Top row: Taiwan; Middle row: Wenchuan; Bottom row: Nepal.

Figure S1

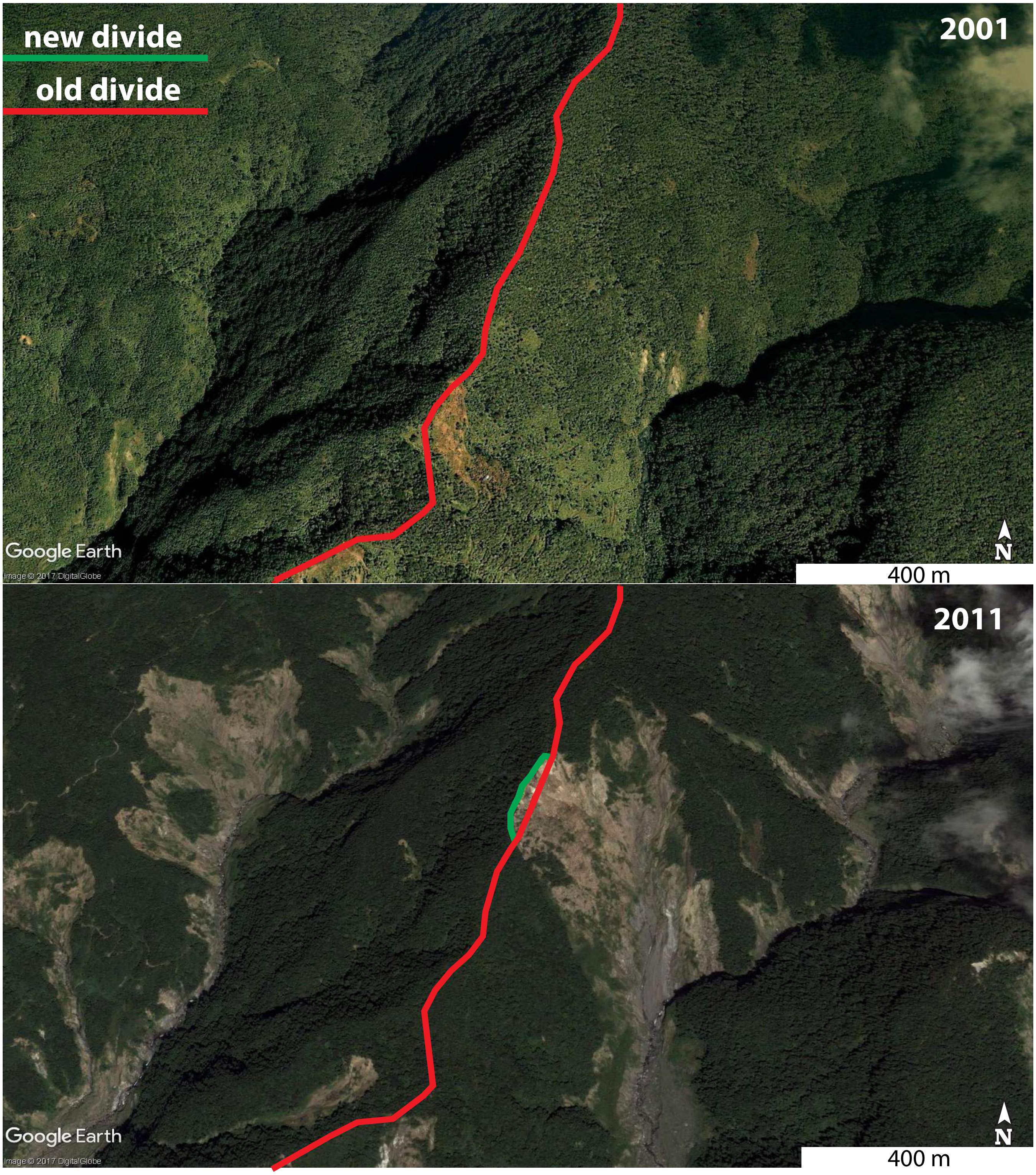
new divide
old divide
2001
Google Earth
Image © 2017 DigitalGlobe
N
400 m
2011
Google Earth
Image © 2017 DigitalGlobe
N
400 m

Figure S2

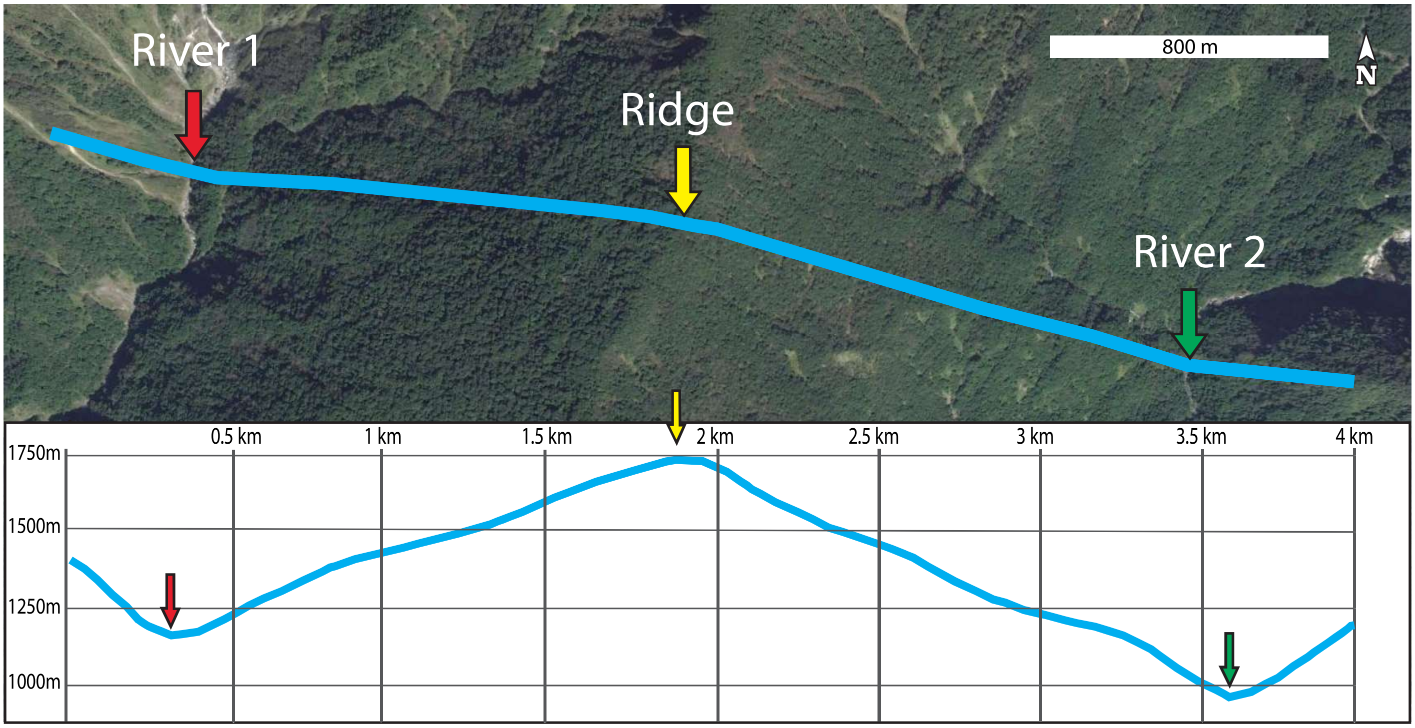

River 1
Ridge
River 2
800 m
N
0.5 km
1 km
1.5 km
2 km
2.5 km
3 km
3.5 km
4 km
1750m
1500m
1250m
1000m

Figure S3

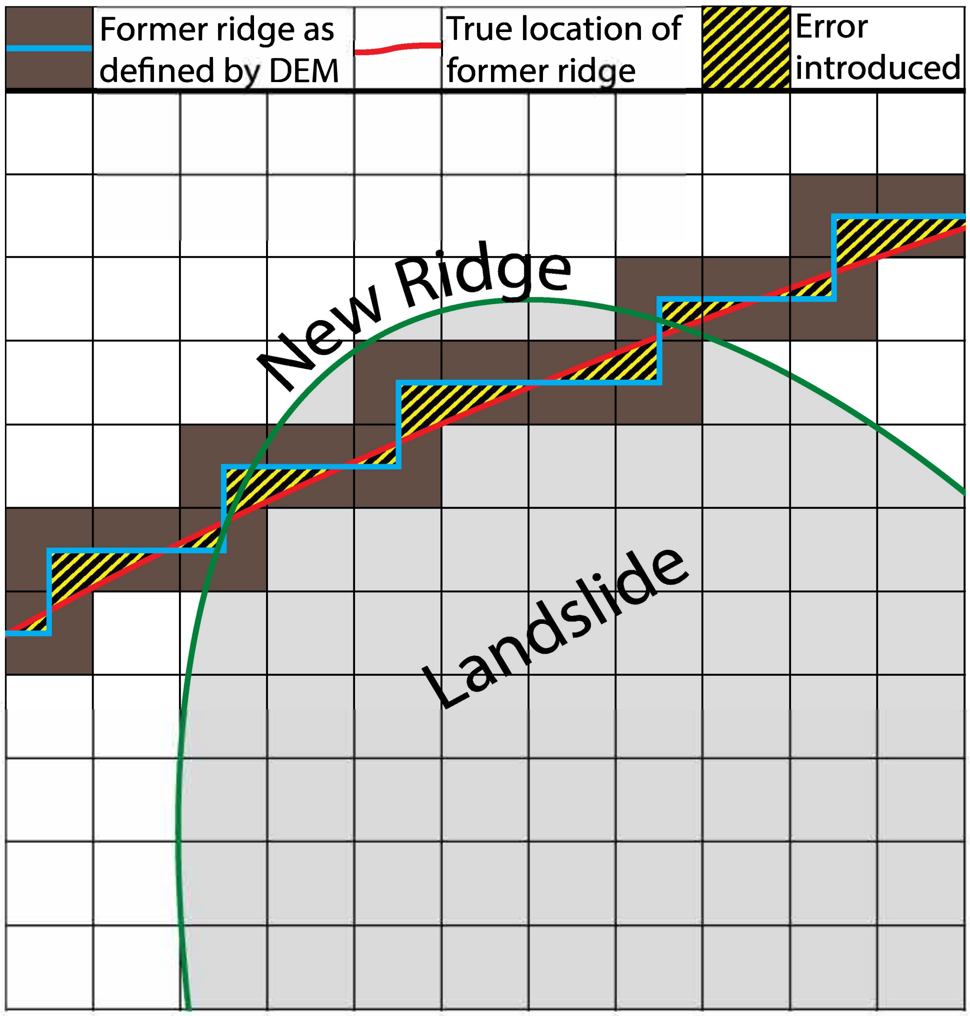

Former ridge as defined by DEM
True location of former ridge
Error introduced
New Ridge
Landslide

Figure S4

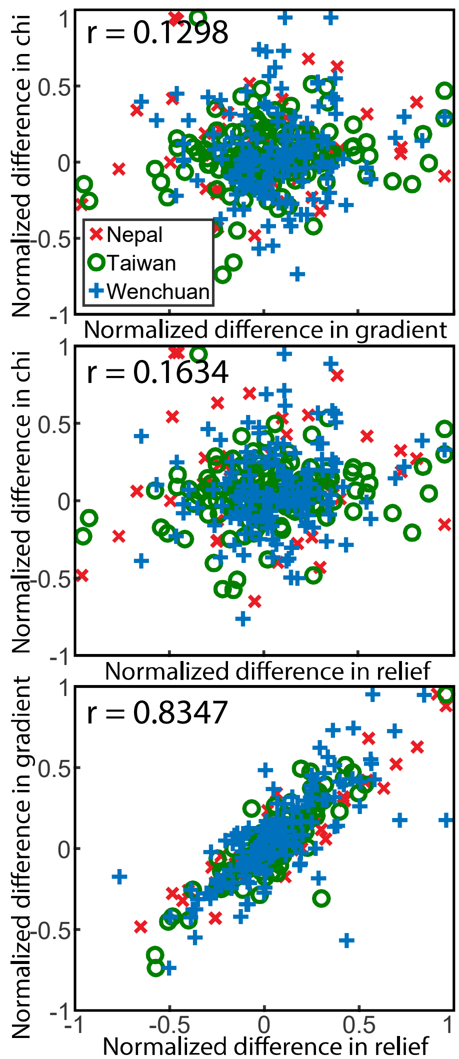
r = 0.1298
Normalized difference in chi
Nepal
Taiwan
Wenchuan
Normalized difference in gradient
r = 0.1634
Normalized difference in chi
Normalized difference in relief
r = 0.8347
Normalized difference in gradient
Normalized difference in relief
1
0.5
0
-0.5
-1
-1
-0.5
0
0.5
1

Figure S5

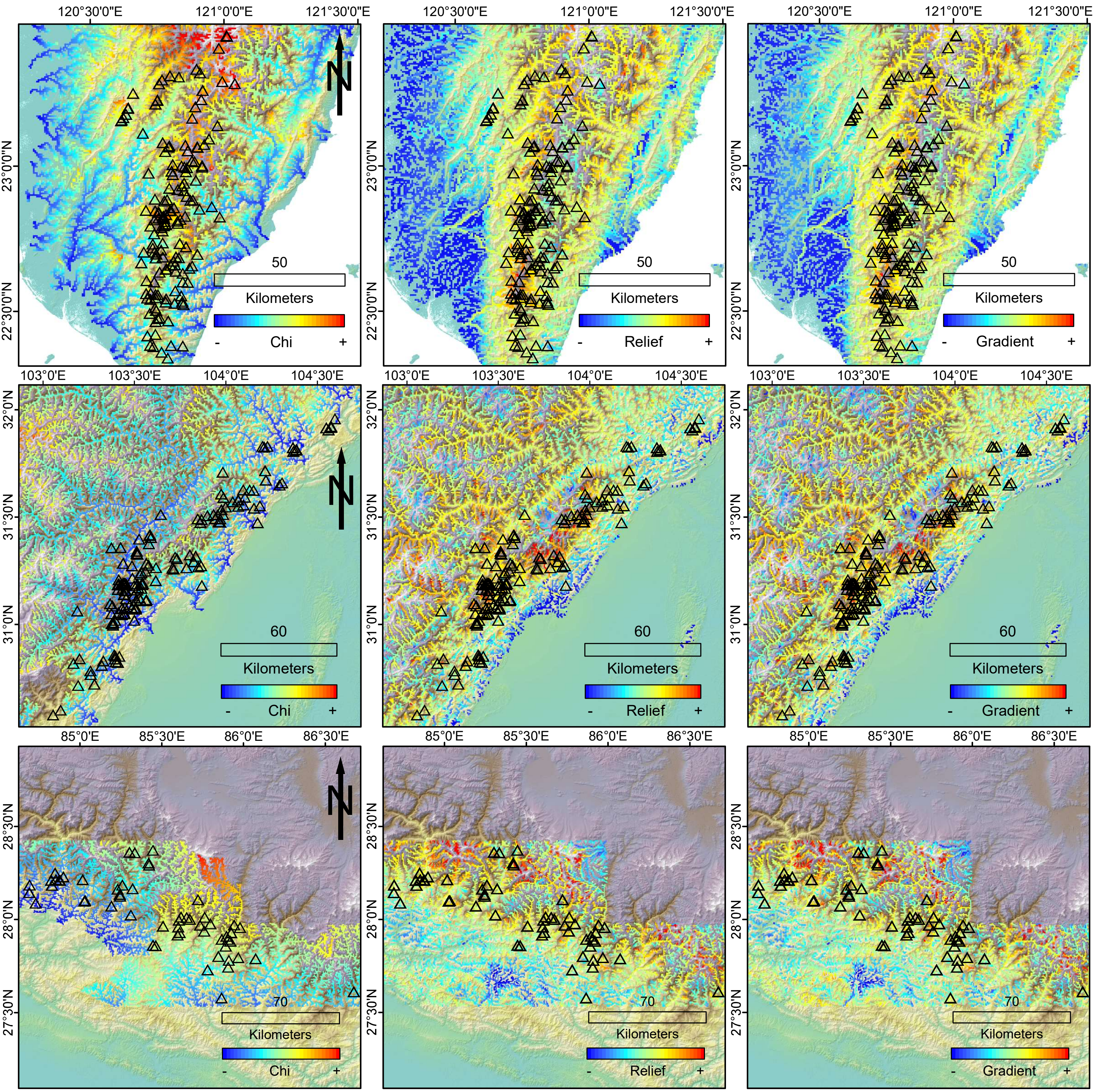
120°30'0"E
121°0'0"E
121°30'0"E
23°0'0"N
22°30'0"N
50
Kilometers
Chi
Relief
Gradient
103°0'E
103°30'E
104°0'E
104°30'E
32°0'N
31°30'N
31°0'N
60
85°0'E
85°30'E
86°0'E
86°30'E
28°30'N
28°0'N
27°30'N
70
N
-
+